physica status solidi a

www.pss-a.com

Tailoring of Magnetic Softness and Magnetoimpedance of Co-Rich Microwires by Stress Annealing

Arcady Zhukov, Lorena Gonzalez-Legarreta, Paula Corte-Leon, Mihail Ipatov, Juan Maria Blanco, Julian Gonzalez, and Valentina Zhukova*

Herein, detailed studies on the influence of stress annealing on the magnetic softness and giant magnetoimpedance (GMI) ratio of $Co_{69.2}Fe_{3.6}Ni_1B_{12.5}Si_{11}Mo_{1.5}C_{1.2}$ glass-coated microwires are provided. As-prepared microwire presents linear hysteresis loops, moderate GMI ratio with double-peak magnetic field dependence and low coercivity (4 A m^{-1}), typically observed for wires with transverse magnetic anisotropy. However, after conventional annealing magnetic hardening and transformation of linear hysteresis loop into rectangular with coercivity about 90 A m^{-1} is surprisingly observed. It is shown that stress annealing allows preventing magnetic hardening and remarkably improving GMI ratio. Properly stress-annealed samples present better magnetic softness: almost unhysteretic loops with coercivity about 2 A m^{-1} and magnetic anisotropy field about 35 A m^{-1}. Observed stress-annealing-induced anisotropy is affected by the tensile stresses, applied during annealing and by the annealing temperature. From the frequency dependence of the maximum GMI ratio, the optimum frequency ranges for as-prepared and stress-annealed samples are determined. The observed stress-annealing-induced magnetic anisotropy and associated changes in magnetic properties and GMI effect are discussed in terms of internal stresses relaxation and related modification of the magnetostriction coefficient, "back stresses," structural anisotropy, redistribution of internal stresses, and change of spatial distribution of magnetic anisotropy.

1. Introduction

Magnetic sensors play an important role in many industries (microelectronics, security and electronic surveillance, automotive, aerospace and aircraft, home entertainment, computer science, electrical engineering, medicine, and so on), providing the ability to detect events, control or monitor various processes and functions, or detect changes in the environment through other electronic devices, for example, through a computer processor.[1–6]

As a rule, the use of magnetic sensors in industries is limited by their cost, sensitivity and dimensionality.[3–6] Accordingly, most modern technologies for measuring magnetic fields require use of magnetically shielded rooms or other systems for active shielding from stray magnetic fields. The other magnetic technologies, e.g., magnetocardiography, can be performed using a superconducting quantum interference device (SQUID).[5,7] However, such technology requires low temperatures to maintain superconductivity as well as magnetic shielding to reduce environmental magnetic noise.[5,7] Accordingly, one of the most relevant trends in the magnetic field monitoring is the development of inexpensive, fast, precise, and effective magnetic field detection method.

Prof. A. Zhukov, P. Corte-Leon, Dr. M. Ipatov, Prof. J. Gonzalez
Dpto. de Polimeros y Materiales Avanzados: Fisica, Quimica y Tecnologia, Fac. Quimica
Universidad del Pais Vasco, UPV/EHU
20018 San Sebastian, Spain
E-mail: arkadi.joukov@ehu.es

The ORCID identification number(s) for the author(s) of this article can be found under https://doi.org/10.1002/pssa.202100130.

DOI: 10.1002/pssa.202100130

Prof. A. Zhukov
IKERBASQUE
Basque Foundation for Science
48011 Bilbao, Spain

Prof. A. Zhukov, P. Corte-Leon, Dr. M. Ipatov, Dr. J. Maria Blanco, Dr. V. Zhukova
Dpto. de Fisica Aplicada, EIG
Universidad del Pais Vasco, UPV/EHU
20018 San Sebastian, Spain

Dr. L. Gonzalez-Legarreta
Dpto. QUIPRE
Nanomedicine-IDIVAL
Inorganic Chemistry-University of Cantabria
Avda. de Los Castros 46, 39005 Santander, Spain

Rather different phenomena can be used for different types of magnetic sensors. Among the phenomena suitable for magnetic field sensors are Hall effect, anisotropic magnetoresistance (AMR), giant magnetoresistance (GMR), tunneling magnetoresistance (TMR), and giant magnetoimpedance (GMI).[5,8–13]

Magnetic and magnetoelastic sensors and smart composites utilizing GMI effect present several advantages such as extremely high sensitivity to external stimuli, as magnetic field, stress or temperature as well as inexpensive technology making them suitable for many applications.[5,7,14–19] The magnetic field sensitivity (up to 10 % A^{-1} m) achieved in magnetic microwires is comparable with those obtained by superconducting quantum interference device, SQUID.[20–22]

The GMI effect consists of a large change in electrical impedance under the action of an applied magnetic field.[12,13,22] The origin of GMI effect as well as the main features of GMI effect have been satisfactorily explained in terms of the skin effect of a soft magnetic conductor considering dependence of skin depth, δ, on applied magnetic field, H.[12,13,20–22] For the case of soft magnetic wire, δ dependence on circumferential magnetic permeability, μ_ϕ, is given as[12,13]

$$\delta = \frac{1}{\sqrt{\pi\sigma\mu_\Phi f}} \tag{1}$$

where σ is the electrical conductivity and f is the AC current frequency. Accordingly, high magnetic permeability is the essential prerequisite for high GMI effect observation.[12,13]

The first GMI effect observation and the best GMI performance are reported for magnetic wires,[20–23] although the GMI effect has been also observed in a vast variety of soft magnetic materials, including ribbons,[24] or thin films.[21]

Typically, the GMI effect is expressed in terms of GMI ratio, $\Delta Z/Z$, given by

$$\frac{\Delta Z}{Z} = \frac{[Z(H) - Z(H_{max})]}{Z(H_{max})} \times 100 \tag{2}$$

The highest (up to 650%) GMI ratio was reported for properly processed amorphous magnetic microwires.[20–22] Several highly sensitive GMI magnetometers and sensors with nT and pT magnetic field sensitivity have been developed.[5,15,17,25] However, theoretically predicted maximum GMI ratio is about 3000% and theoretically estimated skin depth minimum, δ_{min}, is about 0.3 μm.[26,27] Therefore, soft magnetic materials with high μ_ϕ and diameter, d, at least an order of magnitude higher than δ_{min}, i.e., with $d \geq 3$ μm must be suitable for the achievement of substantial GMI ratio.

Accordingly, micrometric amorphous wires with diameters, d, 3–30 μm attract attention as the most promising GMI materials.[20–22,26,27]

Amorphous wires with a wide d range can be prepared by a variety of techniques involving rapid melt quenching: 1) Amorphous wires with $60 \leq d \leq 320$ μm can be prepared using the so called "in-rotating water" method.[5,28] 2) The so-called melt extraction technique allows the fabrication of amorphous wires with $30 \leq d \leq 60$ μm.[29–31] 3) Glass-coated (composite) microwires with metallic nucleus diameters, d, from 185 nm,[32] up to 100 μm,[33] can be obtained by so-called modified Taylor-Ulitovsky (also known as quenching-and-drawing) method known since the 1960s.[34,35]

The latter method allows to vary the diameter of the metallic nucleus of a glass-coated microwire by almost three orders of magnitude, providing the most suitable geometry for GMI materials. Additional advantages of the Taylor-Ulitovsky method are almost continuous preparation method (suitable for the preparation of continuous microwires up to 10 km in length) and the presence of a thin flexible and biocompatible glass coating that allows anticorrosive and mechanical properties improvement and the biocompatibility.[36–38]

Generally, the best magnetic softness is reported in Co-rich amorphous microwires with nearly zero magnetostriction coefficient, λ_s.[20–22,39–41] Such compositional dependence of soft magnetic properties is commonly interpreted by the effect of magnetoelastic anisotropy.[20–22,40–42] The magnetoelastic anisotropy constant, K_{me}, is determined by λ_s and the internal stresses, σ_i.[22,24,25] In amorphous alloys, λ_s is linked with the chemical composition: vanishing λ_s values are observed in Co_xFe_{1-x} $(0 \leq x \leq 1)$ or Co_xMn_{1-x} $(0 \leq x \leq 1)$ for $0.03 \leq x \leq 0.08$.[40–43] The origins of internal stresses are the rapid melt quenching itself and the different thermal expansion coefficients of the metallic nucleus and the glass coating.[44–46] Accordingly, for a given chemical composition (with a specified magnetostriction), the magnetoelastic anisotropy can be further reduced by internal stresses relaxation. The common way for internal stresses relaxation is a thermal treatment.[31,37,39,42]

For that reason, much attention has been drawn to studies of various postprocessing (conventional furnace annealing, Joule heating, or stress annealing) on the magnetic softness and the GMI effect of glass-coated microwires.[20–22,47–54]

Surprisingly, substantial magnetic hardening is observed in various Co-rich microwires after conventional furnace annealing.[55–57] The origin of such magnetic hardening was attributed either to a modification in the magnetostriction coefficient upon annealing due to stresses relaxation, or with the domain structure transformation after heat treatment.[55–57]

Therefore, it is expected that alternative postprocessing such as Joule heating or stress annealing can modify the magnetic anisotropy distribution toward more suitable for a high GMI effect achievement.

There are several reports, where Joule heating has improved the GMI ratio.[20,22] The peculiarity of Joule heating is associated not only with the heating itself, but also with the circumferential magnetic field H_{circ}, created by the current, I, (Oersted field), expressed as [22,58]

$$H_{circ} = I/2\pi r \tag{3}$$

where r is the radial distance. Consequently, the highest H_{circ} is achieved at the surface. Therefore, Joule heating allows annealing in the presence of circumferential magnetic field in the surface layer.[22]

As reported in previous studies,[59–61] magnetic anisotropy of amorphous materials is substantially affected by stresses and/or magnetic field annealing. A macroscopic magnetic anisotropy in

amorphous materials depends on the annealing temperature, stress, and magnetic applied during the annealing.

The beneficial influence of stress annealing on magnetic softness and the GMI effect is also recently reported for Fe-rich microwires with large and positive magnetostriction coefficient.[59,62] The observed modification of hysteresis loops in Fe-rich microwires has been attributed to transverse magnetic anisotropy induced by stress annealing.[59,62] The stress-annealing-induced magnetic anisotropy is proportional to the tensile stress applied during annealing, the annealing temperature and time, and partially recoverable by postannealing.[59,62,63]

In a few recent publications was observed that, although stress-annealed Co-rich microwires generally showed higher coercivity, H_c, than as-prepared Co-rich microwires, they may have a higher GMI ratio.[47–49,51] There are expectations that magnetic hardening previously reported in Co-rich microwires upon annealing can be avoided if conventional annealing will be replaced by stress annealing.

Accordingly, in this article, we provide an overview of the trends related to the optimization of the magnetic softness and the GMI effect of Co-rich glass-coated magnetic microwires by stress annealing, and present some new experimental results on the effect of stress annealing on the magnetic softness and the GMI effect of Co-rich microwires.

2. Experimental Results and Discussion

2.1. Effect of Annealing on Magnetic Properties

2.1.1. Effect of Conventional Furnace Annealing on Magnetic Properties

The hysteresis loops of the as-prepared and annealed in a conventional furnace (without stress) at different temperatures microwires are shown in **Figure 1**. The as-prepared sample presents rather soft magnetic properties with a coercivity, H_c, about $7\,A\,m^{-1}$ and a magnetic anisotropy field, H_k, about $150\,A\,m^{-1}$ (see Figure 1a). These properties are typical for as-prepared Co-rich microwires with vanishing λ_s.[20–22,39–41,56,57]

However, for hysteresis loops of the samples annealed at temperatures between 200 and 400 °C, a remarkable magnetic hardening and transformation of the linear hysteresis loop into rectangular is observed (see Figure 1). Such annealing influence is similar to that observed in previous publications.[56,57] It is interesting that the coercivity grows from $H_c \approx 7\,A\,m^{-1}$ up to $H_c \approx 90\,A\,m^{-1}$ even at the lowest T_{ann} (200 °C). However, the remanent magnetization, M_r/M_o, gradually increases rising T_{ann}, reaching almost $M_r/M_o \approx 1$ (see **Figure 2**).

The commonly accepted core–shell domain structure model of Co-rich magnetic wires implies that their domain structure

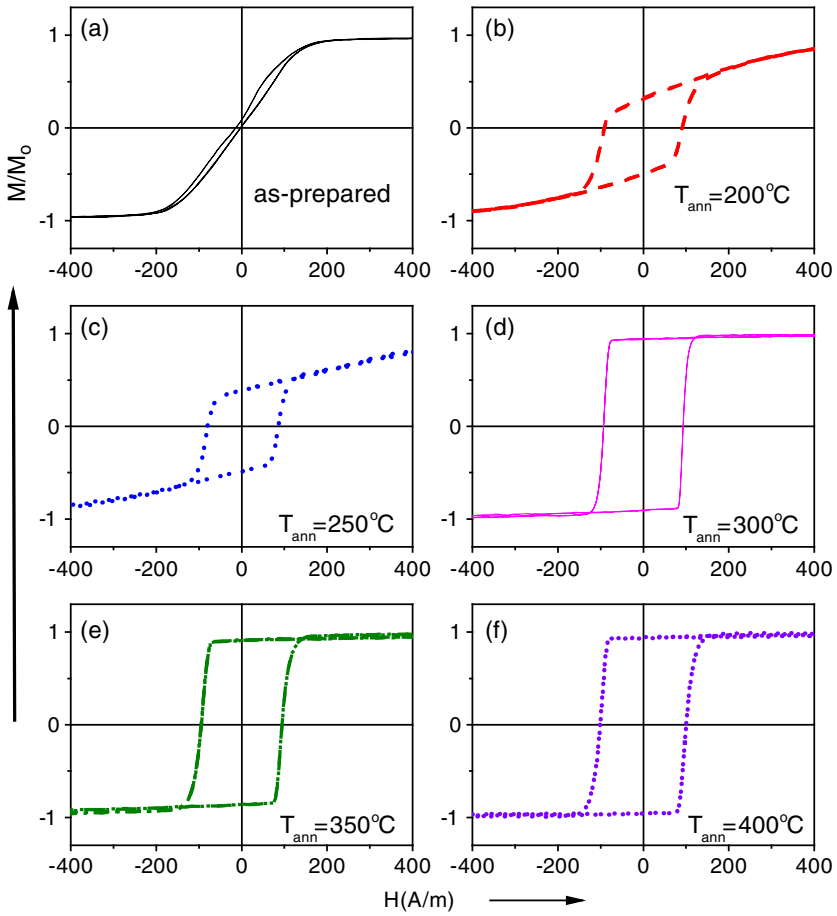

Figure 1. Hysteresis loops of as-prepared and annealed at different temperatures microwires.

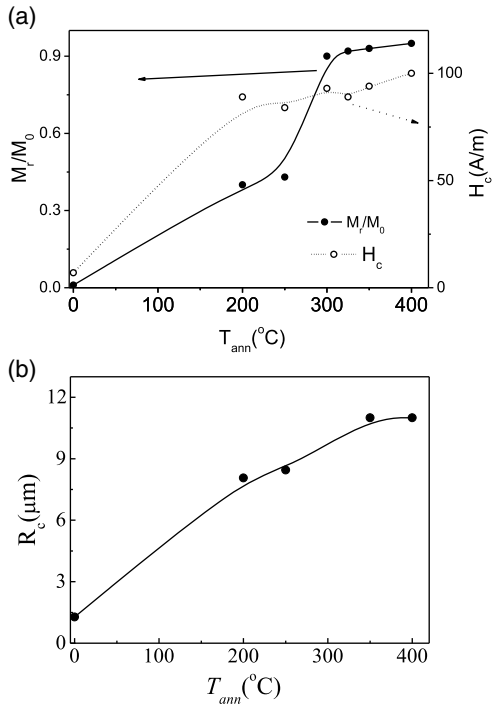

Figure 2. a) Coercivity, H_c, and remanent magnetization, M_r/M_o, dependence on annealing temperature, T_{ann} and b) R_c (T_{ann}) dependence evaluated for the studied microwire. The lines are just guides for eyes.

consists of inner axially magnetized core surrounded by an outer shell with a transverse magnetization orientation.[64,65] From such model, the inner core radius, R_c, can be evaluated from M_r/M_o as

$$R_c = R\sqrt{\frac{M_r}{M_o}} \quad (4)$$

where R is the microwire radius.

As M_r/M_o gradually increases upon annealing (see Figure 2a), increase in R_c rising the annealing temperature is shown in Figure 2b. Therefore, the observed magnetic hardening can be associated with an increase in the inner axially magnetized core radius, R_c, and a corresponding change in the remagnetization process: from the magnetization rotation in the outer domain shell which occupies almost the entire microwire volume, to the magnetization switching in the inner axially magnetized core by a single Barkhausen jump.

Indeed, single domain wall propagation is observed in Co-rich microwires with annealing-induced magnetic bistability.[51,57]

The origin of observed change in the hysteresis loop character, internal stresses relaxation, can be due to negative magnetostriction and predominantly axial internal stresses, which give rise to transverse magnetization orientation and hence transverse magnetic anisotropy of as-prepared Co-rich microwires.[21]

In contrast, annealing affects λ_s due to stress dependence of magnetostriction: an increase in λ_s upon annealing at $T_{ann} \approx 300\,^{\circ}C$ and change from negative to positive λ_s sign are observed for $Fe_{3.6}Co_{69.2}Ni_1B_{12.5}Si_{11}Mo_{1.5}C_{1.2}$ microwire.

Accordingly, conventional annealing of studied microwire gives rise to substantial magnetic hardening and hence more appropriate postprocessing is needed to avoid such magnetic hardening.

2.1.2. Influence of Stress Annealing on Magnetic Properties

As reported in previous studies, stress annealing is a useful tool allowing tuning of magnetic anisotropy of amorphous materials.[59–63] Therefore, stress annealing carried out at different T_{ann} and σ has been evaluated to improve magnetic softness of studied Co-rich microwire.

Several examples are presented in the following paragraphs. Similar to that observed for various Co-rich microwires,[47–50] substantial changes of the hysteresis loops are observed after stress annealing. Such changes are affected by several parameters, like T_{ann} and σ.

Thus, for moderate T_{ann} stress-annealed samples present lower H_c and higher M_r/M_o than the samples annealed at the same T_{ann} (see **Figure 3**). Furthermore, H_c decreases and M_r/M_o increases with increasing σ.

However, this tendency changes with increasing T_{ann}. Thus, at $T_{ann} = 300\,^{\circ}C$, H_c continues to decrease, whereas M_r/M_o begins to decrease with increasing σ (see **Figure 4**a). All stress-annealed samples, at $T_{ann} = 300\,^{\circ}C$, present rectangular hysteresis loops with rather low H_c (Figure 4a). Finally, stress annealing at $T_{ann} = 300\,^{\circ}C$ and $\sigma = 472$ MPa presents $H_c \approx 14\ A\,m^{-1}$ and magnetic anisotropy field, $H_k \approx 50\ A\,m^{-1}$ which is below $H_k \approx 200\ A\,m^{-1}$ observed for as-prepared samples (see a comparison in Figure 4b).

Better magnetic softness of stress-annealed microwire is evidenced from comparison of annealed and stress-annealed ($T_{ann} = 300\,^{\circ}C$ and $\sigma = 472$ MPa) sample (see Figure 4b).

This tendency is even more evident for the microwire annealed at higher T_{ann} ($T_{ann} = 325\,^{\circ}C$): for $\sigma > 354$ MPa a remarkable decrease in H_c and M_r/M_o is observed (see **Figure 5**a). A substantial difference of annealed at $T_{ann} = 325\,^{\circ}C$ and stress-annealed at $T_{ann} = 325\,^{\circ}C$ and $\sigma = 472$ MPa microwires is shown in Figure 5b. Finally, stress annealing at $T_{ann} = 325\,^{\circ}C$ and $\sigma = 472$ MPa allows substantial improvement of magnetic softness: microwires with

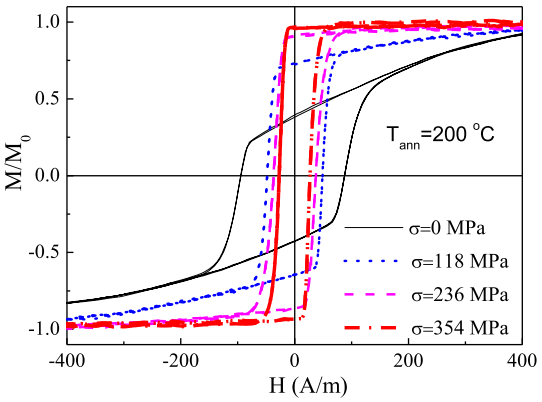

Figure 3. Hysteresis loops of studied microwires annealed and stress annealed at $T_{ann} = 200\,^{\circ}C$.

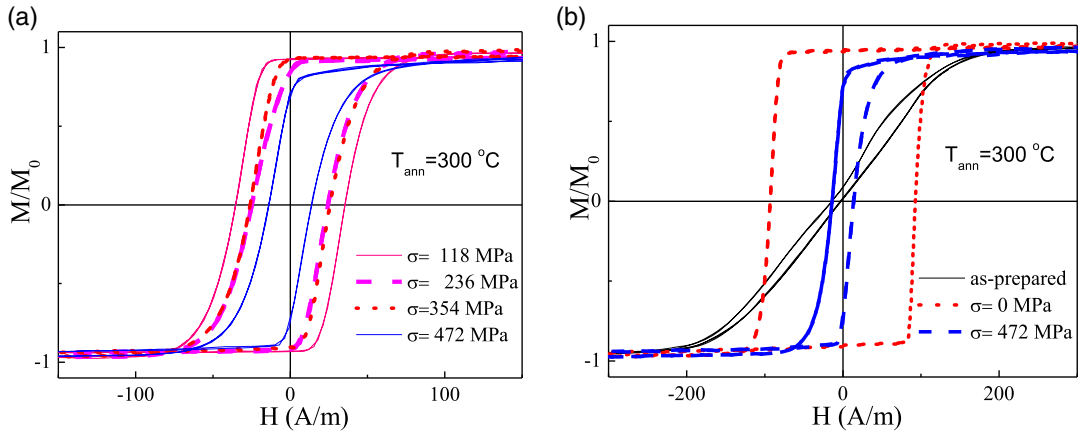

Figure 4. Hysteresis loops of studied microwires a) stress annealed at $T_{ann} = 300\,^{\circ}C$ and b) comparison of hysteresis loops of as-prepared, annealed at $T_{ann} = 300\,^{\circ}C$ and stress-annealed at $T_{ann} = 300\,^{\circ}C$ and $\sigma = 472$ MPa microwires.

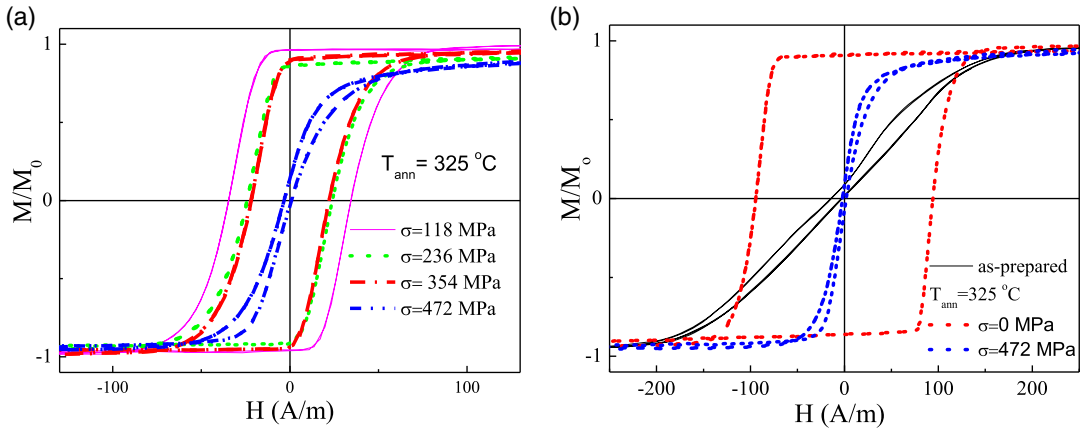

Figure 5. Hysteresis loops of studied microwires a) stress annealed at $T_{ann} = 325\,^{\circ}C$ and different σ and b) comparison of hysteresis loops of as-prepared, annealed at $T_{ann} = 325\,^{\circ}C$ and stress-annealed at $T_{ann} = 325\,^{\circ}C$ and $\sigma = 472$ MPa microwires.

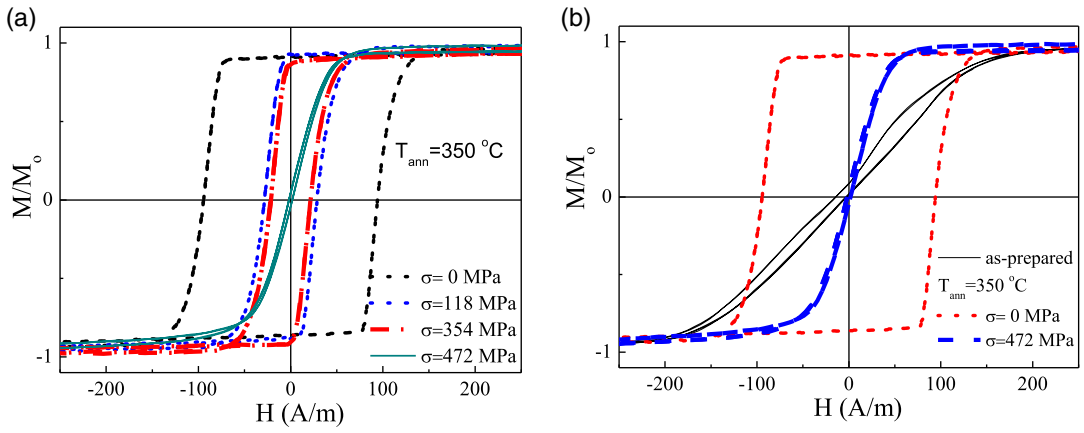

Figure 6. Hysteresis loops of studied microwires a) annealed and stress annealed at $T_{ann} = 350\,^{\circ}C$ and at different σ and b) comparison of hysteresis loops of as-prepared, annealed at $T_{ann} = 350\,^{\circ}C$ and stress annealed at $T_{ann} = 350\,^{\circ}C$ and $\sigma = 472$ MPa microwires.

$H_c \approx 3\ A\ m^{-1}$ and magnetic anisotropy field $H_k \approx 35\ A\ m^{-1}$ have been obtained (see Figure 5a,b). The hysteresis loop of such sample is no more rectangular with vanishing H_c and M_r/M_o.

Even lower $H_c \approx 2\ A\ m^{-1}$ is observed for the sample annealed at $T_{ann} = 350\,^{\circ}C$ ($\sigma = 472$ MPa) (see **Figure 6**). However, in this case, $H_k \approx 50\ A\ m^{-1}$. A remarkable influence of stress applied

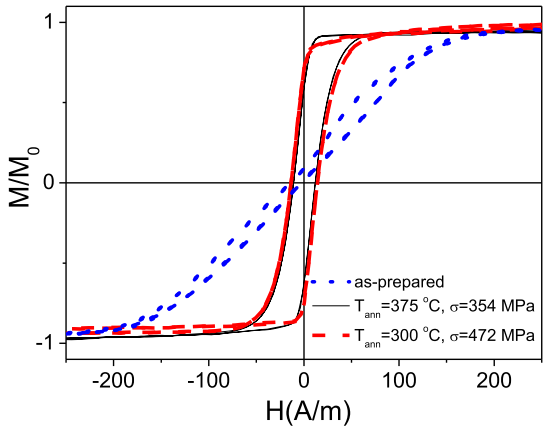

Figure 7. Hysteresis loops of as-prepared microwires and stress annealed at $T_{ann} = 300\,^{\circ}C$, $\sigma = 472$ MPa and $T_{ann} = 375\,^{\circ}C$, $\sigma = 354$ MPa.

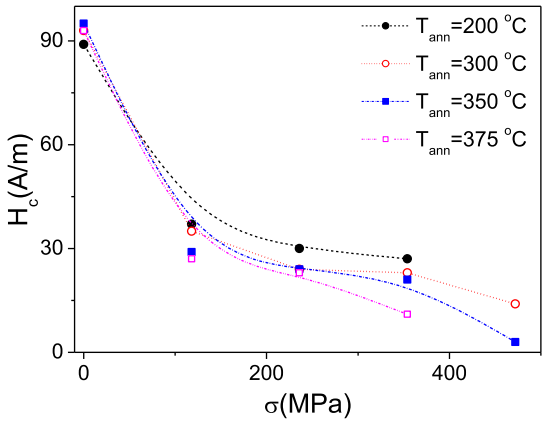

Figure 9. H_c (σ) dependencies evaluated for different T_{ann}.

during the annealing is shown in Figure 6b, which shows the hysteresis loops of annealed and stress-annealed ($T_{ann} = 350\,^{\circ}C$, $\sigma = 472$ MPa) samples.

Accordingly, aforementioned modification of hysteresis loops induced by stress annealing is affected by both T_{ann} and σ. One of the examples shown in **Figure 7** is that almost the same hysteresis loops can be obtained for different T_{ann} and σ. As shown in Figure 7, the samples annealed at $T_{ann} = 300\,^{\circ}C$, $\sigma = 472$ MPa and $T_{ann} = 375\,^{\circ}C$, $\sigma = 354$ MPa present nearly the same magnetic properties, i.e., $H_c \approx 14\ A\ m^{-1}$ and $H_k \approx 50\ A\ m^{-1}$.

Earlier, we have presented all the experimental results (hysteresis loops) measured at fixed T_{ann} and different σ. However, the same tendency: decrease in M_r/M_o and H_c can be observed from measurements presented at fixed $\sigma = 354$ MPa and different T_{ann} (see **Figure 8**).

A tendency of H_c evolution with increase in σ at different T_{ann} is shown in **Figure 9**.

Observed behavior is consistent with features of stress-annealing-induced (also known as creep) magnetic anisotropy in amorphous ribbons,[59–61] and Fe-rich microwires:[58,62] 1) tensile stresses, σ, applied during annealing affect the observed induced anisotropy: for a given temperature/time, induced anisotropy increases with σ increasing; 2) such magnetic anisotropy increases with an increase in the annealing temperature, T_{ann}, at fixed σ.

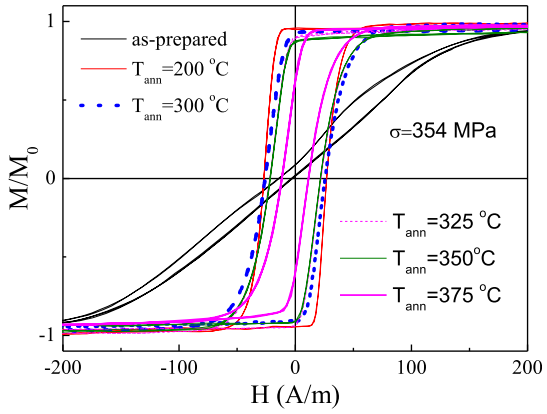

Figure 8. Hysteresis loops of as-prepared microwires and stress annealed at $\sigma = 354$ MPa and different T_{ann}.

Perhaps, the most unusual is that such a significant stress annealing effect is observed for Co-rich microwires with vanishing λ_s. However, the observed effect of stress annealing on the hysteresis loops is rather different from that observed in Fe-rich microwires with high and positive λ_s: the hysteresis loops of Fe-rich microwires change monotonically from rectangular to linear after stress annealing. In addition, the induced anisotropy in Fe-rich is induced easier than that for Co-rich: more substantial hysteresis loops modification can be induced in Fe-rich microwires by stress annealing carried out at the same conditions (T_{ann} and σ).[58,62]

One of the possible origins of such different behavior is different λ_s sign and value. Indeed, it was previously reported that stress-annealing-induced anisotropy depends on the alloy composition, as well as on the magnetostriction.[59–61] The other peculiarity of studied microwire is that after annealing the λ_s sign changes from negative to positive.[51] This fact can explain the change of the tendency observed in $H_c(T_{ann})$ and $M_r/M_o(T_{ann})$ dependencies upon stress annealing (see **Figure 10**a,b): both $H_c(T_{ann})$ and $M_r/M_o(T_{ann})$ dependencies demonstrate a monotonic increase in H_c and M_r/M_o with T_{ann} for $\sigma = 0$ MPa. This tendency changes at sufficiently high T_{ann} and σ. Stress-annealed microwires present lower H_c –values. In addition, $H_c(T_{ann})$ dependence shows a decrease in H_c for $T_{ann} \geq 200\,^{\circ}C$ for all σ (see Figure 10a). Similarly, at $T_{ann} \geq 200\,^{\circ}C$ and $\sigma = 354$ MPa a change in the $M_r/M_o(T_{ann})$ dependence is observed (see Figure 10b).

The origin of stress-induced anisotropy in various amorphous materials is previously discussed in terms of either "back stresses," directional pair (chemical or topological) atomic ordering or structural anisotropy.[58–63]

The most common origin of stress- or magnetic field-annealing-induced anisotropy is pair ordering mechanism.[60] However, stress- or field-annealing-induced anisotropy is observed even in a single magnetic element-based amorphous alloys, i.e., in Fe based.[58,60,62,66]

Therefore, a contribution of the glass former, i.e., boron, in the directional ordering, or as an "interstitial," is proposed.[60,66]

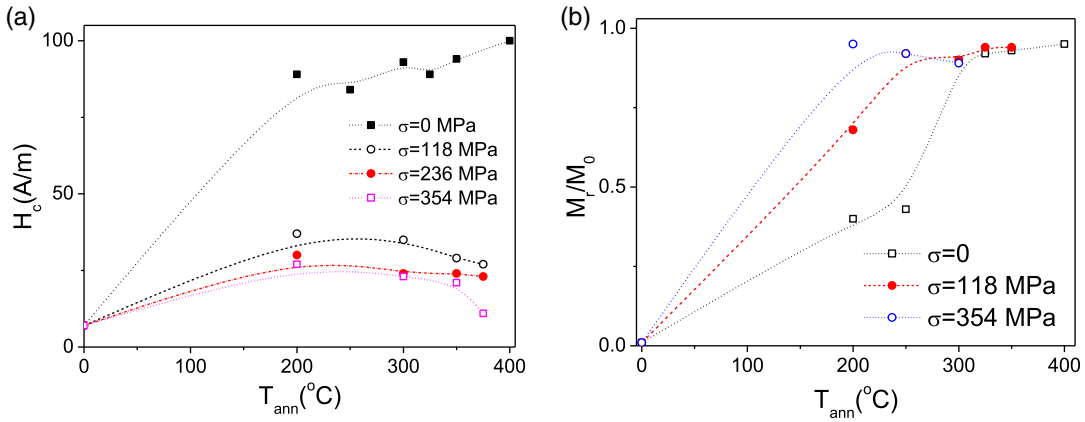

Figure 10. a) H_c (T_{ann}) and b) M_r/M_o (T_{ann}) dependencies evaluated for different σ.

In addition, explanation of stress-annealing-induced anisotropy as a structural anisotropy either originated by residual bond anisotropy after removing the external stress or by a residual strain is proposed.[61,67]

Such stress-annealing-induced magnetic anisotropy can be partially or completely recovered by subsequent annealing.[61,63,67]

The magnetic properties, like, e.g., coercivity, H_c, are quite sensitive to the strain due to the magnetoelastic anisotropy. Therefore, λ_s sign and value are one among the relevant parameters that can affect features of stress-annealing-induced magnetic anisotropy.

Achieved remarkable magnetic softening can affect GMI performance of the studied microwires. Therefore, the experimental results on the effect of stress annealing on the GMI ratio of the studied microwires are provided in the following sections.

2.2. Effect of Annealing on GMI Effect

2.2.1. GMI Effect in as-Prepared Microwires

As-prepared sample presents moderate GMI effect ($\Delta Z/Z_{max}$ up to 100%) and double-peak $\Delta Z/Z(H)$ dependencies in a whole range of frequencies, f (see **Figure 11**a).

From $\Delta Z/Z_{max}(f)$, evaluated from $\Delta Z/Z(H)$ dependencies measured at different frequencies, one can see that the optimum frequency at which reaches a maximum (about 102%) is 80 MHz (see Figure 11b).

As stress annealed at appropriate conditions samples can present better magnetic softness, better GMI properties are expected for stress-annealed samples. Experimental results on GMI effect in stress-annealed samples are provided in the following sections.

2.2.2. Effect of Stress Annealing on GMI Effect of Studied Microwires

Better magnetic softness has been achieved in stress annealed at 300 °C $\leq T_{ann} \leq$ 375 °C samples. Consequently, following text presented the GMI performance of these samples.

A remarkable GMI ratio improvement is observed in all stress annealed (at $\sigma = 472$ MPa) Co-rich microwires (see comparison in **Figure 12**a–c): all stress-annealed (at $\sigma = 472$ MPa) samples present more than double GMI ratio improvement with $\Delta Z/Z_{max}$ above 200%.

In addition, stress annealing also affects the shape of $\Delta Z/Z(H)$ dependencies: although all stress-annealed samples present double-peak $\Delta Z/Z(H)$ dependence (see Figure 12a–c),

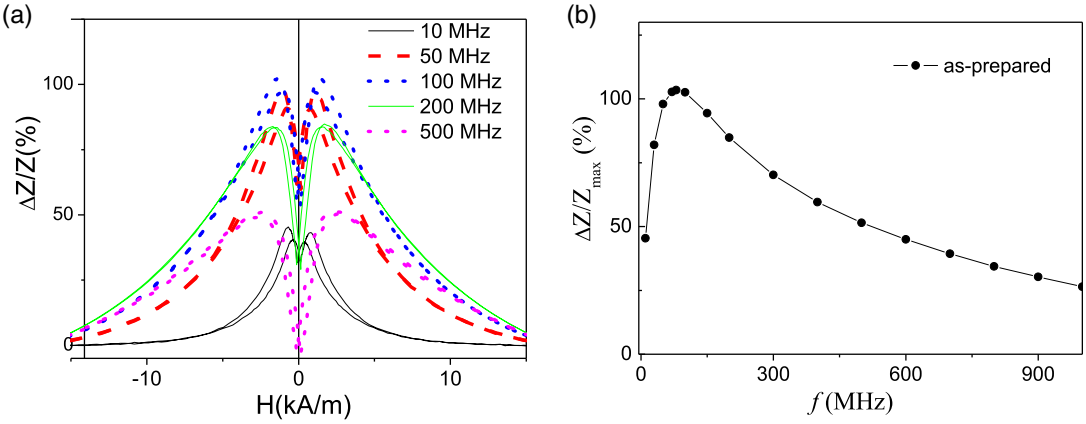

Figure 11. a) $\Delta Z/Z(H)$ dependencies measured at different frequencies and b) $\Delta Z/Z_{max}(f)$ evaluated for as-prepared sample.

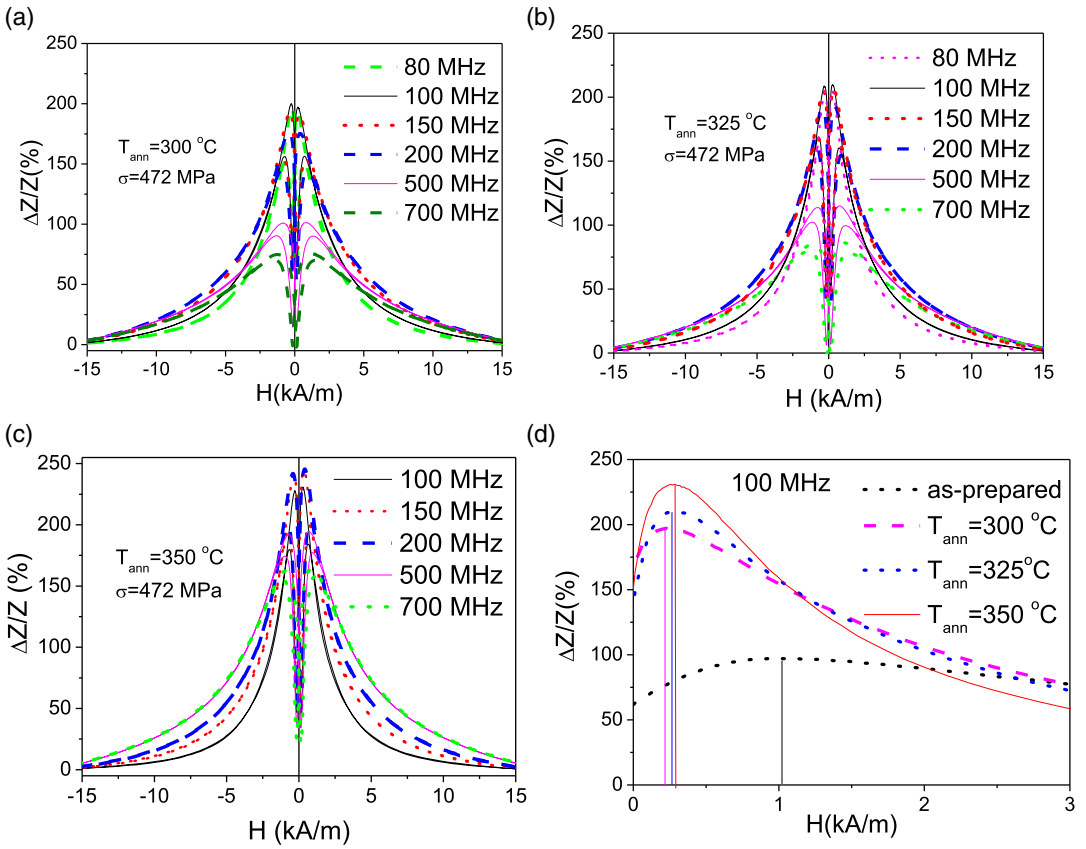

Figure 12. $\Delta Z/Z(H)$ dependencies of stress annealed ($\sigma = 472$ MPa) measured at different frequencies for a) $T_{ann} = 300\,^{\circ}C$, b) $T_{ann} = 325\,^{\circ}C$, c) $T_{ann} = 350\,^{\circ}C$, and d) a comparison of $\Delta Z/Z(H)$ dependencies of as-prepared and stress-annealed ($\sigma = 472$ MPa) $f = 100$ MHz.

the magnetic field at which the maximum on $\Delta Z/Z(H)$ dependence takes place, H_m, becomes lower than that for the as-prepared sample. From a comparison of $\Delta Z/Z(H)$ dependencies of as-prepared and stress annealed ($\sigma = 472$ MPa, $f = 100$ MHz), this difference in H_m is clearly observed (see Figure 12d). Furthermore, slight increase in H_m –values with increase in T_{ann} from 300 to 350 °C can be appreciated. As discussed in previous studies, H_m is linked to magnetic anisotropy field.[12,21]

Higher H_m values as-compared with H_k evaluated from bulk hysteresis loops (see Figure 6 and 7) must be attributed to spatial distribution of magnetic anisotropy and higher magnetic anisotropy in the surface. As reported in previous studies, skin depth, δ, for $f = 100$ MHz in Co-rich microwires is generally below 1–2 μm, being about an order of magnitude lower than the microwire radius.[49,68]

Therefore, the observed stress-annealing influence on $\Delta Z/Z(H)$ dependencies correlates with the evolution of the hysteresis loops upon stress annealing and hence can be associated to stress-annealed-induced magnetic anisotropy.

A comparison of $\Delta Z/Z_{max}(f)$ dependencies for as-prepared and stress-annealed samples is shown in **Figure 13**. Superior $\Delta Z/Z_{max}$ values for all the frequency ranges (up to 1 GHz) are evident for stress-annealed samples as-compared with as-prepared sample.

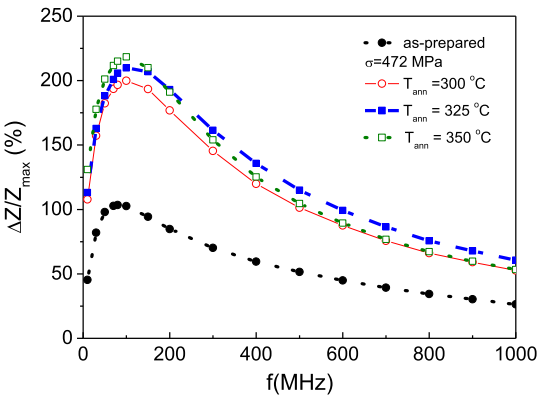

Figure 13. $\Delta Z/Z_{max}(f)$ dependencies for as-prepared and stress-annealed samples.

It is worth noting that the optimum frequency for as-prepared sample is about 80 MHz, however, for stress-annealed samples, the optimal frequency shifts to about 150 MHz. The $\Delta Z/Z_{max}$ ratios of stress-annealed samples are quite similar (of about 220%). For, $f \leq 200$ MHz, the highest $\Delta Z/Z_{max}$ ratio is observed for $T_{ann} = 350\,^{\circ}C$, whereas for $f \geq 200$ MHz, slightly higher $\Delta Z/Z_{max}$ ratio is observed for $T_{ann} = 325\,^{\circ}C$.

Consequently, we can resume that the stress-induced anisotropy allows tuning of both the GMI ratio value and the $\Delta Z/Z_{max}(f)$ dependencies.

3. Conclusion

The impact of stress annealing on soft magnetic properties and the giant magnetoimpedance effect of $Co_{69.2}Fe_{3.6}Ni_1B_{12.5}Si_{11}Mo_{1.5}C_{1.2}$ glass-coated microwire is studied.

As-prepared microwire presents linear hysteresis loops, moderate GMI ratio, and low coercivity (4 A m^{-1}). However, after conventional annealing a substantial magnetic hardening and transformation of linear hysteresis loop into rectangular with coercivity about 90 A m^{-1} are observed.

We have showed that stress annealing allows preventing magnetic hardening and remarkably improving GMI ratio in the frequency range up to 1 GHz. Appropriately stress-annealed samples present better magnetic softness with almost unhysteretic loops with coercivity about 2 A m^{-1} and magnetic anisotropy field about 35 A m^{-1}.

Observed stress-annealing-induced anisotropy is affected by the tensile stresses, applied during annealing, in such a way that for a given annealing temperature, induced anisotropy increases with stresses increasing. In addition, such magnetic anisotropy increases with an increase in the annealing temperature at fixed stress.

The optimum frequency range for as-prepared and stress-annealed samples is determined from the frequency dependence of the maximum GMI ratio.

The origin of stress-annealing-induced magnetic anisotropy has been discussed in terms of internal stresses relaxation and related modification of the magnetostriction coefficient, "back stresses", structural anisotropy, redistribution of internal stresses, and change of spatial distribution of magnetic anisotropy.

4. Experimental Section

As mentioned earlier, magnetostriction coefficient and magnetic properties of glass-coated microwires were substantially affected by both chemical composition and geometry (metallic nucleus diameters, d, total microwire diameter, D, and ratio $\rho = d/D$). Therefore, we studied glass-coated microwires with fixed $Co_{69.2}Fe_{3.6}Ni_1B_{12.5}Si_{11}Mo_{1.5}C_{1.2}$ composition and geometry ($d = 22.8$ μm, $D = 23.2$ μm) prepared using the Taylor-Ulitovsky method.

The preparation method (commonly denominated as the Taylor-Ulitovsky technique) of glass-coated metallic microwires consisted of the controllable casting of long (up to few km long continuous microwires), homogeneous, rather thin and composite (metallic nucleus covered by thin glass coating) wires of micrometric diameters.[21,34,44,69]

In the laboratory process, the master alloy was placed into a Pyrex-like glass tube and heated by a high-frequency inductor heater up to melting, followed by casting of composite (metallic nucleus covered by thin glass coating) microwire. Then, a glass capillary was drawn from a softened glass portion, capturing a metallic alloy, and then wound on a rotating bobbin (see **Figure 14**a). Accordingly, under suitable casting conditions, a composite microwire was formed, in which the metal nucleus was completely covered with a glass sheath (see Figure 14b).[69]

Roughly, 1 km of microwire required 1 g of metallic alloy ingot.[69] One of the advantages of glass-coated microwires was that the insulating and flexible glass coating provides several functionalities, like better anticorrosion and mechanical properties.

Amorphous structure of as-prepared $Fe_{3.6}Co_{69.2}Ni_1B_{12.5}Si_{11}Mo_{1.5}C_{1.2}$ microwire was proved by X-ray diffraction (XRD) using a BRUKER (D8 Advance) X-ray diffractometer with Cu K_α ($\lambda = 1.54$ Å) radiation. As-prepared $Co_{69.2}Fe_{3.6}Ni_1B_{12.5}Si_{11}Mo_{1.5}C_{1.2}$ microwire presented XRD patterns with broad halo typical for completely amorphous materials. The beginning of crystallization was observed after annealing at annealing temperature, $T_{ann} = 490$ °C for 60 min.

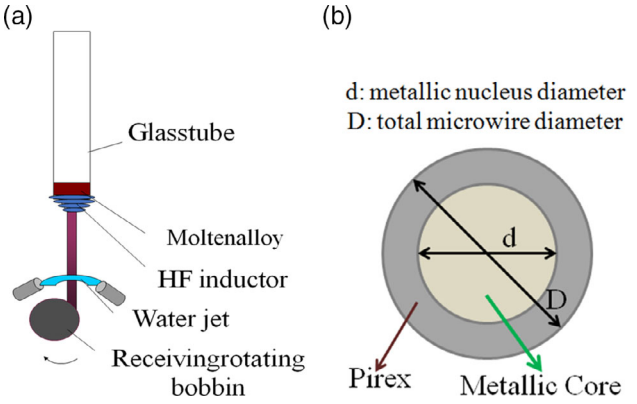

Figure 14. a) Schematic picture of the Taylor-Ulitovsky method allowing preparation of glass-coated microwires and b) cross section of a microwire. Reproduced with permission.[69] Copyright 2017, MDPI.

The magnetostriction coefficient, λ_s, determined by the small-angle magnetization rotation (SAMR) method gave value $\lambda_s \approx -0.3 \times 10^{-6}$.[49]

We have studied as-prepared and annealed samples. All the samples were annealed in a conventional furnace at temperatures, T_{ann}, up to 400 °C with fixed annealing time, t_{ann}, (60 min). In the case of stress annealing, the tensile stress, σ, was applied during the annealing and was removed only after the sample cooling with the furnace. The σ value within the metallic nucleus was evaluated considering different Young's moduli of the metal and the glass as described in previous studies.[47–50] The maximum σ value used in this study was 472 MPa.

The fluxmetric method, described in detail in previous studies,[49] was used to evaluate the hysteresis loops, which were plotted as the normalized magnetization, M/M_0, versus magnetic field, H, being M—the magnetic moment at given magnetic field and M_0—the magnetic moment at the maximum magnetic field amplitude, H_m. While H_c and remanent magnetization, M_r/M_0, were evaluated directly from hysteresis loops, the magnetic anisotropy field, H_k, was defined from hysteresis loop as the crossing point of linear extrapolations of low-field magnetization curve and saturation curve as previously described in previous studies.[70]

The sample impedance, Z, was evaluated from the reflection coefficient S_{11} using the vector network analyzer. We used a microstrip sample holder placed inside a long solenoid that creates a homogeneous magnetic field, H, as described in details in previous studies.[39] Described technique allowed measuring the GMI effect in extended frequency, f, range up to GHz frequencies. The GMI ratio was obtained using Equation (2). Maximum GMI ratio, $\Delta Z/Z_{max}$, obtained from $\Delta Z/Z(H)$ dependencies as a maximum $\Delta Z/Z$ value. $\Delta Z/Z_{max}$ was a useful characteristic for comparison of the samples subjected to different postprocessing (annealing).[21,22,39]

Acknowledgements

This work was supported by the Spanish MCIU, under PGC2018-099530-B-C31 (MCIU/AEI/FEDER, UE), and by the Government of the Basque Country, under PIBA 2018-44 and Elkartek (CEMAP and AVANSITE) projects, and by the University of Basque Country, under the scheme of "Ayuda a Grupos Consolidados" (Ref.: GIU18/192) and COLAB20/15 project. The authors are thankful for the technical and human support provided by SGIker of UPV/EHU (Medidas Magnéticas Gipuzkoa) and European funding (ERDF and ESF).

Conflict of Interest

The authors declare no conflict of interest.

Data Availability Statement

Research data are not shared.

Keywords

annealing, giant magnetoimpedance, internal stresses, magnetic microwires, magnetoelastic anisotropy

Received: March 9, 2021
Revised: April 8, 2021
Published online: April 29, 2021

[1] J. Lenz, A. S. Edelstein, *IEEE Sens J.* **2006**, *6*, 631.
[2] M. Díaz-Michelena, *Sensors* **2009**, *9*, 2271.
[3] E. A. Vitol, V. Novosad, E. A. Rozhkova, *Nanomedicine* **2012**, *7*, 1611.
[4] P. Ripka, G. Vertesy, *J. Magn. Magn. Mater.* **2000**, *215*, 795.
[5] K. Mohri, T. Uchiyama, L. V. Panina, M. Yamamoto, K. Bushida, *J. Sens.* **2015**, *2015*, 718069.
[6] D. C. Jiles, *Acta Mater.* **2003**, *51*, 5907.
[7] J. Ma, Z. Yang, T. Uchiyama, *AIP Adv.* **2019**, *9*, 125243,
[8] A. Karsenty, *Sensors* **2020**, *20*, 4163.
[9] C. Zheng, K. Zhu, S. Cardoso de Freitas, J.-Y. Chang, J. E. Davies, P. Eames, P. P. Freitas, O. Kazakova, C. G. Kim, C.-W. Leung, S.-H. Liou, A. Ognev, S. N. Piramanayagam, P. Ripka, A. Samardak, K.-H. Shin, S.-Y. Tong, M.-J. Tung, S. X. Wang, S. Xue, X. Yin, P. W. T. Pong, *IEEE Trans. Magn.* **2019**, *55*, 0800130.
[10] M. N. Baibich, J. M. Broto, A. Fert, F. Nguyen Van Dau, F. Petron, P. Etienne, G. Creuzer, A. Friederich, J. Chazelas, *Phys. Rev. Lett.* **1988**, *61*, 2472.
[11] J. Inoue, S. Maekawa, *Phys. Rev. B* **1996**, *53*, R11927.
[12] L. V. Panina, K. Mohri, *Appl. Phys. Lett.* **1994**, *65*, 1189.
[13] R. S. Beach, A. E. Berkowitz, *Appl. Phys. Lett.* **1994**, *64*, 3652.
[14] D. Karnaushenko, D. D. Karnaushenko, D. Makarov, S. Baunack, R. Schäfer, O. G. Schmidt, *Adv. Mater.* **2015**, *27*, 6582.
[15] T. Uchiyama, K. Mohri, Sh. Nakayama, *IEEE Trans. Magn.* **2011**, *47*, 3070.
[16] A. F. Cobeño, A. Zhukov, J. M. Blanco, V. Larin, J. Gonzalez, *Sens. Actuator, A* **2001**, *91*, 95.
[17] L. Ding, S. Saez, C. Dolabdjian, L. G. C. Melo, A. Yelon, D. Ménard, *IEEE Sens. J.* **2009**, *9*, 159.
[18] M. Ipatov, G. R. Aranda, V. Zhukova, L. V. Panina, J. González, A. Zhukov, *Appl. Phys. A* **2011**, *103*, 693.
[19] D. Makhnovskiy, A. Zhukov, V. Zhukova, J. Gonzalez, *Adv. Sci. Tech.* **2008**, *54*, 201.
[20] K. R. Pirota, L. Kraus, H. Chiriac, M. Knobel, *J. Magn. Magn. Mater.* **2000**, *21*, L243.
[21] A. Zhukov, M. Ipatov, P. Corte-León, L. Gonzalez-Legarreta, M. Churyukanova, J. M. Blanco, J. Gonzalez, S. Taskaev, B. Hernando, V. Zhukova, *J. Alloys Compd.* **2020**, *814*, 152225.
[22] P. Corte-León, V. Zhukova, M. Ipatov, J. M. Blanco, J. Gonzalez, A. Zhukov, *Intermetallics* **2019**, *105*, 92.
[23] E. P. Harrison, G. L. Turney, H. Rowe, *Nature* **1935**, *135*, 961.
[24] L. V. Panina, K. Mohri, T. Uchiyama, M. Noda, K. Bushida, *IEEE Trans. Magn.* **1995**, *31*, 1249.
[25] S. Gudoshnikov, N. Usov, A. Nozdrin, M. Ipatov, A. Zhukov, V. Zhukova, *Phys. Status Solidi A* **2014**, *211*, 980.
[26] L. Kraus, *J. Magn. Magn. Mater.* **1999**, *195*, 764.
[27] M. Ipatov, V. Zhukova, A. Zhukov, J. Gonzalez, A. Zvezdin, *Phys. Rev. B* **2010**, *81*, 134421.
[28] M. Hagiwara, A. Inoue, T. Masumoto, *Metall. Trans.* **1982**, *13A*, 373.
[29] P. Rudkowski, G. Rudkowska, J. O. Strom-Olsen, *Mater. Sci. Eng. A* **1991**, *133*, 158.
[30] V. Zhukova, A. Zhukov, V. Kraposhin, A. Prokoshin, J. Gonzalez, *Sens. Actuator, A* **2003**, *106*, 225.
[31] J. S. Liu, F. Y. Cao, D. W. Xing, L. Y. Zhang, F. X. Qin, H. X. Peng, X. Xue, J. F. Sun, *J. Alloys Compd.* **2012**, *541*, 215.
[32] T.-A. Ovári, N. Lupu, H. Chiriac, *Rapidly Solidified Magnetic Nanowires and Submicron Wires in Advanced Magnetic Materials*, INTECH Open Access Publisher, Rijeka, Croatia **2012**, pp. 1–32.
[33] P. Corte-Leon, V. Zhukova, M. Ipatov, J. M. Blanco, J. González, M. Churyukanova, S. Taskaev, A. Zhukov, *J. Alloys Compd.* **2020**, *831*, 150992.
[34] A. V. Ulitovsky, I. M. Maianski, A. I. Avramenco, USSR Patent 128427, Bulletin No. 10, **1960**.
[35] L. Kraus, J. Schneider, H. Wiesner, *Czech. J. Phys. B* **1976**, *26*, 601.
[36] T. Goto, M. Nagano, N. Wehara, *Trans. JIM* **1977**, *18*, 759.
[37] V. Zhukova, A. F. Cobeño, A. Zhukov, A. R. de Arellano Lopez, S. López-Pombero, J. M. Blanco, V. Larin, J. Gonzalez, *J. Magn. Magn. Mater.* **2002**, *249*, 79.
[38] D. Kozejova, L. Fecova, P. Klein, R. Sabol, R. Hudak, I. Sulla, D. Mudronova, J. Galik, R. Varga, *J. Magn. Magn. Mater.* **2019**, *470*, 2.
[39] A. Zhukov, M. Ipatov, P. Corte-Leon, J. M. Blanco, L. González-Legarreta, V. Zhukova, *IEEE Instr. Meas. Mag.* **2020**, *23*, 56.
[40] Y. Konno, K. Mohri, *IEEE Trans. Magn.* **1989**, *25*, 3623.
[41] M. Churyukanova, V. Semenkova, S. Kaloshkin, E. Shuvaeva, S. Gudoshnikov, V. Zhukova, I. Shchetinin, A. Zhukov, *Phys. Status Solidi A* **2016**, *213*, 363.
[42] G. Herzer, in *Proc. of the NATO Advanced Study Institute on Magnetic Hysteresis in Novel Materials*, NATO ASI Series (Series E: Applied Sciences), vol. *338* (Ed.: G. C. Hadjipanayis), Kluwer Academic Publishers, Dordrecht/Boston/London, **1997**, pp. 711-730.
[43] A. F. Cobeño, A. Zhukov, J. M. Blanco, J. Gonzalez, *J. Magn. Magn. Mater.* **2001**, *234*, L359.
[44] S. A. Baranov, V. S. Larin, A. V. S. Torcunov, *Crystals* **2017**, *7*, 136.
[45] V. Zhukova, J. M. Blanco, M. Ipatov, A. Zhukov, *Phys. B* **2012**, *407*, 1450.
[46] H. Chiriac, T.-A. Ovari, *J. Magn. Magn. Mater.* **2002**, *249*, 46.
[47] V. Zhukova, M. Ipatov, A. Talaat, J. M. Blanco, M. Churyukanova, A. Zhukov, *J. Alloys Compd.* **2017**, *707*, 189.
[48] V. Zhukova, P. Corte-Leon, M. Ipatov, J. M. Blanco, L. Gonzalez-Legarreta, A. Zhukov, *Sensors* **2019**, *19*, 4767.
[49] L. Gonzalez-Legarreta, P. Corte-Leon, V. Zhukova, M. Ipatov, J. M. Blanco, J. Gonzalez, A. Zhukov, *Sensors* **2020**, *20*, 1558.
[50] D. González-Alonso, L. González-Legarreta, P. Corte-León, V. Zhukova, M. Ipatov, J. M. Blanco, A. Zhukov, *Sensors* **2020**, *20*, 3227.
[51] L. Gonzalez-Legarreta, P. Corte-León, V. Zhukova, M. Ipatov, J. M. Blanco, M. Churyukanova, S. Taskaev, A. Zhukov, *J. Alloys Compd.* **2020**, *830*, 154576.
[52] J. Liu, F. Qin, D. Chen, H. Shen, H. Wang, D. Xing, M.-H. Phan, J. Sun, *J. Appl. Phys.* **2014**, *115*, 17A326.
[53] H. Chiriac, T.-A. Óvári, *IEEE Trans. Magn.* **2002**, *38*, 3057.
[54] K. R. Pirota, L. Kraus, H. Chiriac, M. Knobel, *J. Magn. Magn. Mater.* **2001**, *226–230*, 730.
[55] A. Zhukov, K. Chichay, A. Talaat, V. Rodionova, J. M. Blanco, M. Ipatov, V. Zhukova, *J. Magn. Magn. Mater.* **2015**, *383*, 232.
[56] A. Zhukov, A. Talaat, M. Churyukanova, S. Kaloshkin, V. Semenkova, M. Ipatov, J. M. Blanco, V. Zhukova, *J. Alloys Compd.* **2016**, *664*, 235.

[57] A. Zhukov, A. Talaat, J. M. Blanco, M. Ipatov, V. Zhukova, *J. Electr. Mater.* **2014**, *43*, 4532.
[58] V. Zhukova, J. M. Blanco, M. Ipatov, J. Gonzalez, M. Churyukanova, A. Zhukov, *Scr. Mater.* **2018**, *142*, 10.
[59] M. Ohnuma, G. Herzer, P. Kozikowski, C. Polak, V. Budinsky, S. Koppoju, *Acta Mater.* **2012**, *60*, 1278.
[60] F. E. Luborsky, J. L. Walter, *IEEE Trans. Magn.* **1977**, *13*, 953.
[61] J. Haimovich, T. Jagielinski, T. Egami, *J. Appl. Phys.* **1985**, *57*, 3581.
[62] V. Zhukova, J. M. Blanco, P. Corte-Leon, M. Ipatov, M. Churyukanova, S. Taskaev, A. Zhukov, *Acta Mater.* **2018**, *155*, 279.
[63] P. Corte-Leon, V. Zhukova, J. M. Blanco, M. Ipatov, S. Taskaev, M. Churyukanova, J. Gonzalez, A. Zhukov, *J. Alloys Compd.* **2021**, *855*, 157460.
[64] M. Vázquez, D.-X. Chen, *IEEE Trans. Magn.* **1995**, *31*, 1229.
[65] V. Zhukova, J. M. Blanco, A. Chizhik, M. Ipatov, A. Zhukov, *Front. Phys.* **2018**, *13*, 137501.
[66] J. J. Becker, *IEEE Trans. Magn.* **1978**, *14*, 938.
[67] P. Kozikowski, M. Ohnuma, R. Hashimoto, K. Takano, G. Herzer, M. Kuhnt, Ch. Polak, *Phys. Rev. Mater.* **2020**, *4*, 095604.
[68] A. Zhukov, A. Talaat, M. Ipatov, A. Granovsky,V. Zhukova, *J. Sci. Adv. Mater. Dev.* **2016**, *1*, 388.
[69] A. Zhukov, M. Ipatov, A. Talaat, J. M. Blanco, B. Hernando, L. Gonzalez-Legarreta, J. J. Suñol, V. Zhukova, *Crystals* **2017**, *7*, 41.
[70] A. Zhukov, J. Gonzalez, J. M. Blanco, M. J. Prieto, E. Pina, M. Vazquez, *J. Appl. Phys.* **2000**, *87*, 1402.